Journal Name

ARTICLE

Structural reorganization in a hydrogen-bonded organic framework

Received 00th January 20xx,
Accepted 00th January 20xx

DOI: 10.1039/x0xx00000x

www.rsc.org/

Javier Castells-Gil,[a] Natalia M. Padial[a] and Carlos Martí-Gastaldo*,[a]

Self-recognition of 3,3',5,5'-azobenzenetetracarboxylic acid drives the formation of a grid-like anionic hydrogen-bonded framework with channels occupied by organic cations. This supramolecular solid is capable of reorganizing its connectivity in the presence of specific guests into a different crystalline architecture by sequential dissolution and recrystallization.

Introduction

Crystal engineering of molecular solids has been pivotal to the tremendous advance in the design of functional frameworks with properties such as porosity, catalysis, ion exchange, proton transport, luminescence or magnetism. This has been well illustrated for crystalline porous solids like Metal-Organic Frameworks (MOFs)[1] and Covalent Organic Frameworks (COFs),[2] for which the spatial distribution of molecular components within a porous structure dictates the properties of the material.

In turn, Hydrogen-bonded Organic Frameworks (HOFs) are based exclusively on the assembly of organic blocks by supramolecular non-covalent interactions. Purely organic crystals offer important advantages like straightforward synthesis, solvent processability, ease of regeneration by recrystallization or low molecular weight.[3-6] Compared to MOFs and COFs based on robust coordination and covalent bonds, H-bonds are weaker, and the resulting structures feature lower chemical and structural stability. This is a key drawback for their use as porous materials. Although there are previous examples demonstrating the ability of supramolecular frameworks to maintain their structural integrity upon solvent removal,[7-16] thermal activation often results in the collapse of the architecture for complete loss of porosity. Unlike their rigid counterparts, that more often can retain the original structure upon guest exchange or solvent removal, HOFs are more flexible and can undergo controlled structural changes based on the directionality of H-bonds and their ability to break and re-form cooperatively in presence of specific guests. Hence, their main source of instability can be used as an asset to access dynamic responses which are not accessible to more robust frameworks. This process is favoured by the lability of the supramolecular interactions that interconnect the components to enable molecular recognition processes for dynamic equilibria between supramolecular architectures. We report an anionic 2D hydrogen-bonded framework built from carboxylic acid supramolecular dimers that features 1D channels covered in H-bond acceptor sites. This provides a chemically adaptable environment capable of reorganizing its connectivity in the presence of other molecular components to form different H-bonded networks. Our results suggest that dynamic self-assembly is controlled by effective interplay of the supramolecular interactions between the host and the cationic guest, that are responsible for the crystallization of a different framework topology.

Experimental Section

Materials and Methods

5-nitroisophthalic acid (98%), guanidine hydrochloride, 98% (GND·HCl) and aminoguanidine hydrochloride, 99% (AmGND·HCl) were purchased from Sigma-Aldrich and used as received. *N,N*-Dimethylformamide (≥ 99.8%) and propan-2-ol (≥ 99.9%) were purchased from Scharlab. Ultrapure water from Milli-Q equipment was used when required. All reagents and solvents were used without any previous purification unless specified. Carbon, nitrogen and hydrogen contents were determined by microanalytical procedures using a LECO CHNS. Infrared spectra were recorded in an Agilent Cary 630 FTIR Spectrometer directly with no need of KBr pellets. Thermogravimetric analysis were carried out with a Mettler Toledo TGA/SDTA 851 apparatus between 25 and 800 °C under ambient conditions (10 °C·min^{-1} scan rate and an air flow of 30 mL·min^{-1}). ^{1}H and ^{13}C NMR spectra were run on a Bruker DRX500 spectrometer. XRD patterns were collected in a PANalytical X'Pert PRO diffractometer using copper radiation (Cu Kα = 1.5418 Å) with an X'Celerator detector, operating at 40 mA and 45 kV. Profiles were collected in the 2° < 2θ < 40° range with a step size of 0.017°. PXRD was collected in a PANalytical

[a] Instituto de Ciencia Molecular, Universitat de València, Catedrático José Beltrán 2, 46980, Paterna (Spain).

Electronic Supplementary Information (ESI) available: [details of any supplementary information available should be included here]. See DOI: 10.1039/x0xx00000x

X'Pert PRO diffractometer using copper radiation (Cu Kα = 1.5418 Å) with an X'Celerator detector, operating at 40 mA and 45 kV. Profiles were collected in the 2° < 2θ < 40° range with a step size of 0.017°.

Synthesis of 3,3',5,5'-azobenzenetetracarboxylic acid (H_4abtc)

H_4abtc was synthesized according to a reported method.[17] In a typical procedure, 5-nitroisophtalic acid (19 g) and sodium hydroxide (50 g) were suspended in 250 mL of Milli-Q water and reacted at 60 °C with continuous stirring for 1 hour. Next, glucose (100 g) was dissolved in 100 mL of warm water and the resulting solution was added dropwise to the yellow slurry that became dark brown due to reduction of the nitro groups. The mixture was left to cool down for 30 minutes followed by exposure to an air stream for 16 hours with continuous stirring at room temperature. Next, the crude was cooled in an ice bath prior to isolation of the solid by filtration with vacuum. Finally, the solid was dissolved in 250 mL of water and acidified with HCl 37% to produce an orange precipitate. This was isolated by filtration, thoroughly washed with water and dried in an oven (92% yield). Elemental analysis for $C_{16}H_{10}N_2O_8$: Calc. C (53.64), H (2.81), N (7.86); found: C (52.59), H (3.02), N (7.75). Spectroscopic data matched those quoted in the bibliography.[18]

Synthesis of $[H_2abtc][DMA]_2$ (1)

H_4abtc (229.3 mg; 0.64 mmol) was suspended in 4 mL of DMF:*i*-PrOH (8:2) in a rubber-lined capped glass vial. The orange suspension was heated up to 150 °C at a rate of 0.2 °C·min^{-1}, held for 48 hours and allowed to cool down at a rate of 0.4 °C·min^{-1}. This results in the formation of orange crystals that were isolated by filtration and rinsed with 45 mL of DMF (3x15 mL) and 45 mL of *i*-PrOH (3x15 mL). The product was dried in a desiccator under vacuum at room temperature. Yield: 69.5%. Elemental analysis for $[C_{16}H_8N_2O_8][(CH_3)_2NH_2]_2$: Calc. C (53.57), H (5.39), N (12.49); found: C (53.57), H (5.12), N (12.55%). ^{1}H-NMR (500 MHz, DMSO-d_6): 8.65 (t, *J = 1.4 Hz*, 2H), 8.52 (d, *J = 1.4 Hz*, 4H), 2.56 (s, 12H). ^{13}C NMR (125 MHz, DMSO-d_6, DEPT) δ: 167.5 (C), 151.4 (C), 136.0 (C), 132.2 (CH), 125.1 (CH), 33.7 (CH_3).

Synthesis of $[H_2abtc][GND]_2{\cdot}2H_2O$ (2)

100 mg of compound **1** were soaked in 5 ml of a guanidine hydrochloride solution in ethanol (96%) and allowed to stand at room temperature for several weeks refreshing the solution every day. After two weeks, single-crystals of **2** suitable for single-crystal X-ray diffraction were obtained. (*See ESI SI2 for NMR data*).

Recrystallization in the presence of different cations

For each time, 15 mg of compound **1** was soaked in 5 mL equimolar solutions of GND·HCl and AmGND·HCl (0.05 mol·L^{-1}, respectively) in ethanol (96%). The solution was refreshing every day during 60 days. After that, the orange solid was washed with 5 mL of absolute ethanol for 3 times, the solvent was removed by syringe and air drying.

Single-Crystal X-ray Diffraction

Suitable crystals of **1** and **2** were selected, mounted on a Mitagen micromont by using paraffin oil and measured on a SuperNova, Single source at offset, Sapphire3 diffractometer. The crystal was kept at 120.00(10) K during data collection. The structure was solved in Olex2[19] by using the ShelXT[20] structure solution program using Intrinsic Phasing and refined with the ShelXL[21] refinement package using Least Squares minimisation.

Results and Discussion

Synthesis and structure of $[H_2abtc][DMA]_2$

3,3',5,5'-azobenzenetetracarboxylic acid (H_4abtc; $C_{16}H_{10}N_2O_8$) was synthesised according to a reported method.[18] This organic molecule displays four exodentate functionalities in a rectangular planar disposition (C_{2h} symmetry) well-suited to direct self-assembly in two dimensions (Figure 1). Reaction of H_4abtc in a mixture of *N,N*-dimethylformamide and propan-2-ol at 150 °C yields $[H_2abtc][DMA]_2$ (DMA^+= dimethylammonium) (**1**). Compound **1** crystallizes in the triclinic space group *P-1* as orange, prismatic crystals of around 100 µm in size. It is built from partially deprotonated H_2abtc^{2-} linkers forming H-bonded syn-syn C=O···H-O carboxyl dimer synthons, sitting at centrosymmetrically related positions. The d(D-A) distances range from 2.465(2) to 2.476(2) Å, values characteristic of strong ionic H-bonds (Table SI4), similar to those reported for other H-bonded organic frameworks.[22-25] Packing of the anionic grid-like layers is controlled by strong π–π stacking between neighbouring aromatic rings. The rings feature a parallel offset arrangement with inter-centroid distances close to 3.5 Å (Figure SI20). As shown in Figure 2, this results in the formation of a layered structure that displays 1D channels along the [100] direction that are occupied by DMA^+ cations for overall charge balance, which originate from decarbonylation of DMF at 150 °C. These are linked to the organic framework by weaker N-H···O=C H-bonds with the central amine group (2.7 Å). The presence of organic cations was also demonstrated by ^{1}H NMR for polycrystalline samples. NMR spectrum of **1** in DMSO confirms the presence of two DMA^+ molecules per H_2abtc linker, consistent with the structural study (Figure SI1). FT-IR spectrum endorses the presence of the characteristic vibrational modes of DMA^+ and aromatic C-H groups in the organic linker (Figure SI10). Phase purity of the bulk material was proved by X-ray powder diffraction (Figure SI14).

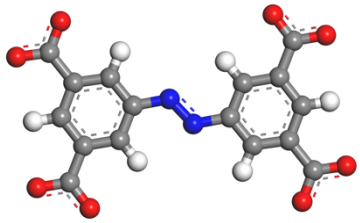

Figure 1. Structure of $abtc^{4-}$.

Thermal stability and structural changes with temperature and exposure to solvents

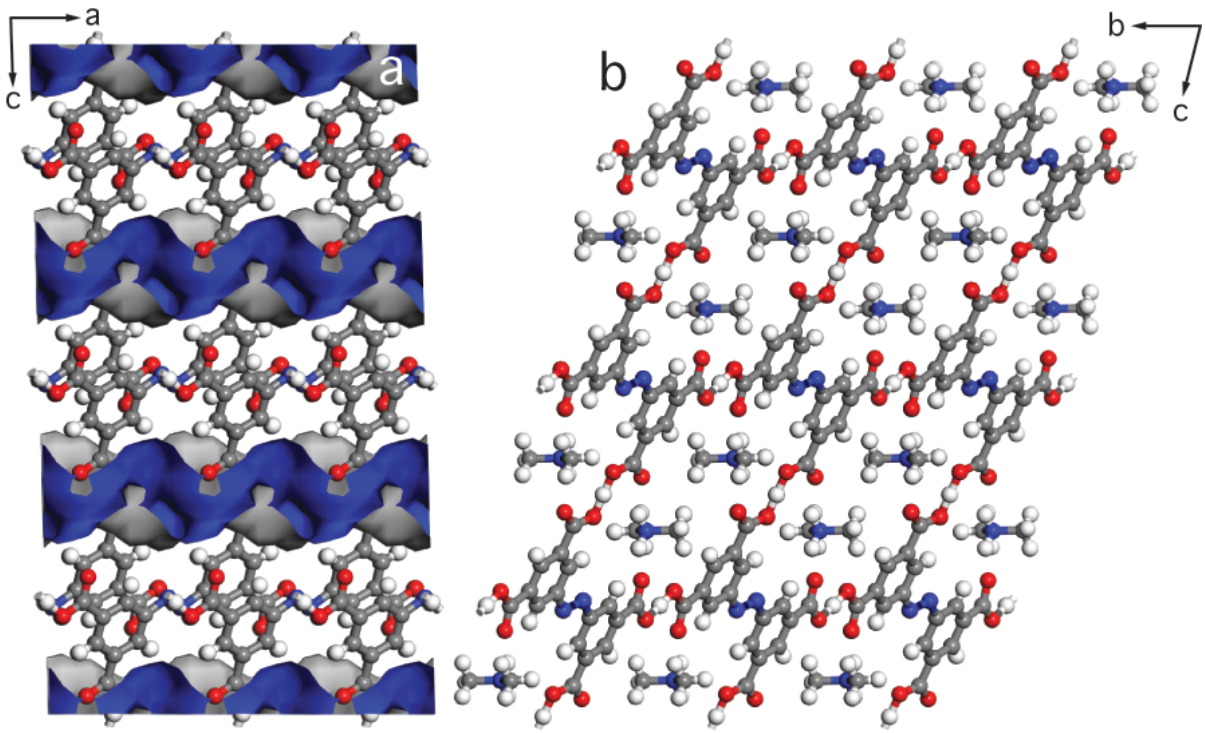

Figure 2. Structure of $[H_2abtc][(DMA]_2$. Interlayer packing results in 1D channels (a) that are occupied by DMA^+ cations interleaved between the grid-like anionic layers (b).

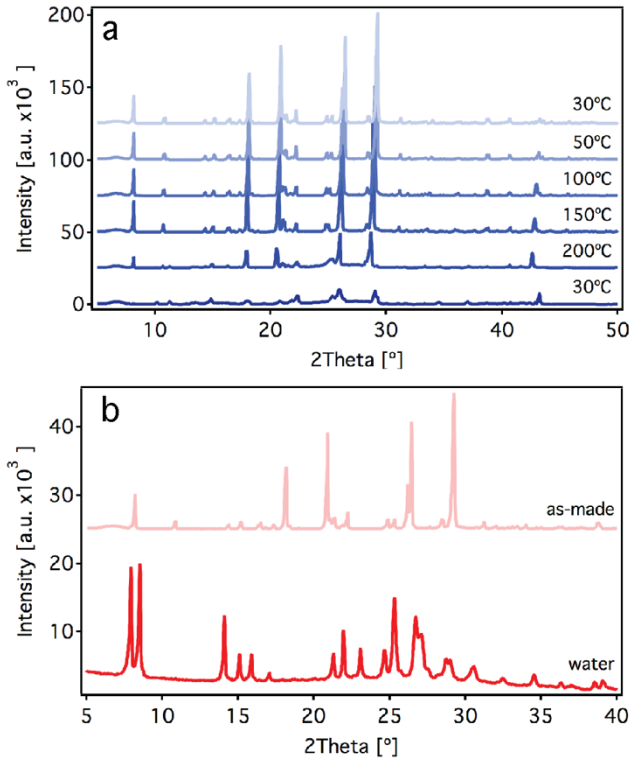

Figure 3. (a) Variable-temperature PXRDs of **1** at 30-200 °C suggesting progressive compression of the unit cell alongside non-reversible amorphization close to 200 °C. See Figure SI22 for unit cell refinement. (b) Crystalline conversion into a different phase upon water exposure.

As shown in Figure SI15, thermogravimetric analysis confirms that the solid is stable up to 200 °C where it shows a first weight loss of 20.4% close to 240 °C, that coincides with the loss of two molecules of DMA. Decomposition of the remaining anion is likely related to the gradual decomposition of the framework that extends from 350 °C to the highest temperature measured. This behaviour is similar to previously reported ionic cation/anion hydrogen-bonded frameworks, with decompositions taking place between 240 and 300 °C.[23]

Figure 3a shows the variable-temperature PXRDs collected between 30-200 °C. **1** undergoes slight compression upon heating, close to 6% in volume according to the refinement of the unit cell form experimental data (Figure SI22). This is accompanied by progressive amorphization that becomes more drastic at 200 °C. The collapse of the structure is non-reversible. Exposure of the amorphous solid to an atmosphere rich in water promoted the formation of a different crystalline phase (Figure 3b). FT-IR suggested the presence of water molecules (Figure SI12) due to the broad band observed around 3400 cm^{-1}. This is also confirmed by the thermal decomposition of this crystalline phase that displays a similar profile than **1** except for the low-temperature regime, with a first weight loss below 100 °C of about 33% that likely corresponds to the release of water molecules (Figure SI18). Though we repeatedly tried to isolate this new phase by modifying the synthetic conditions, we did not manage to isolate single crystals that enable to elucidate the structure of this phase. However, the weight loss step at 240 °C corresponding to the loss of dimethylamine molecules is lower than that calculated for the release of two dimethylamine molecules (Calc: 15.1%, Exp: 8.5) which suggests a partial decomposition of the framework upon exposure to water.

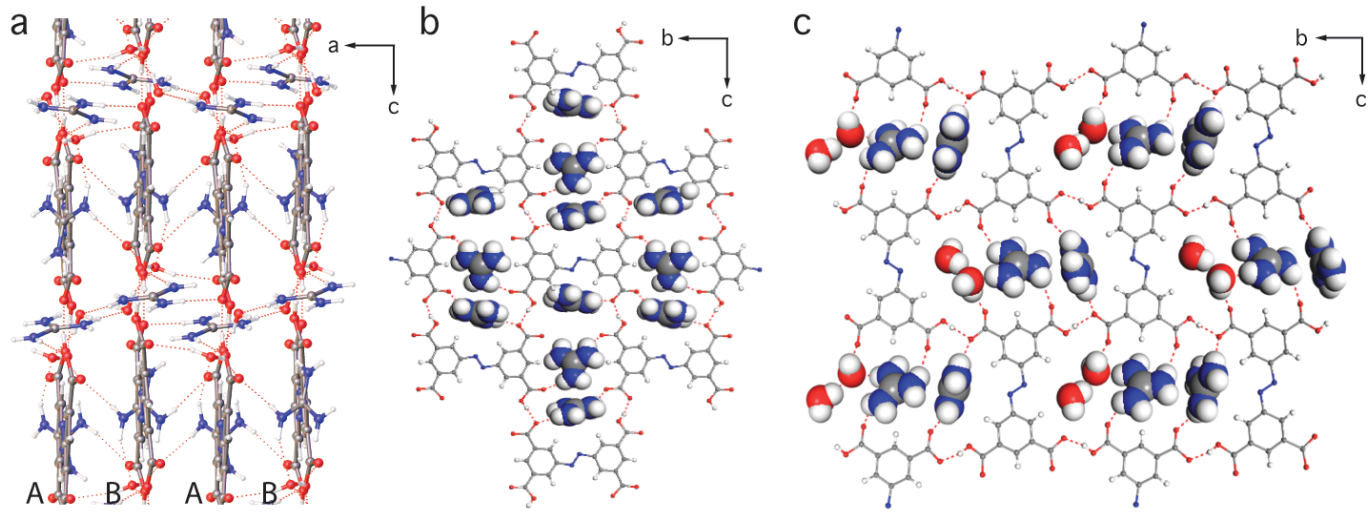

Figure 4. Structure of $[H_2abtc][GND]_2 \cdot EtOH$. (a) Packing of the layers following a ..ABAB.. sequence. (b) Internal structure of the layers accommodating GND^+ cations in the cavities via H-bond with H_2abtc^{2-}. (c) Inclusion of solvent molecules disrupts 2D connectivity in type-A layers for the formation of 1D zig-zag segregated chains.

Although very small in our case, this structural flexibility is not surprising for HOFs. Ionic H-bonds combine sufficient strength and directionality to endow the framework with the flexibility necessary to adapt its structure to solvent removal or guest inclusion.[23,26-28] Compared to the structural changes in water, **1** retains its original structure when soaked in DMF and organic solvents like EtOH or *i*-PrOH and slightly changes in MeOH (Figure SI23), with minimum changes in the chemical composition or the IR spectrum of the final solid. This suggests that structural reorganization might be linked to the use of solvents with high hydrogen bond donation (HBD) ability. The observed behaviour coincides with the trend of HBD values calculated by stepwise multiple linear regression for these solvents: H_2O > MeOH > EtOH > *i*-PrOH > DMF.[29] We argued this selective structural response could be also extended to the incorporation of other cations to the structure of **1**.

Crystallization of $[H_2abtc][GND]_2 \cdot 2H_2O$

We selected guanidinium (GND^+) and aminoguanidinium ($AmGND^+$) cations because their size is slightly bigger than DMA^+ and have three and four H-bonding donor sites compared to only one in DMA^+. As-made crystals of **1** were soaked in saturated ethanolic solutions of the chloride salts of GND^+ and $AmGND^+$ separately (0.1 and 0.05 $mol \cdot L^{-1}$) and left to stand in static conditions with continuous refreshing of the solutions every 24 hours. After one week GND^+ triggers the formation of crystals of $[H_2abtc][GND]_2 \cdot 2H_2O$ (**2**) with a different morphology (Figure SI9). Formation of the inclusion complex seems to follow the procedure of an addition of GND^+ to the pre-organized DMA^+ network, that might induce a self-assembly equilibrium between both cations towards the selective formation of a specific supramolecular architecture with lower solubility. Similar dynamic exchanges between molecular components have been reported for supramolecular architectures in solution.[26,27,30] No single-crystals could be obtained when $AmGND^+$ was employed likely due to the higher dilution imposed by the lower solubility of this salt.

2 crystallizes in the centrosymmetric $P2_1/c$ space group. Similar to **1**, there is one crystallographically independent H_2abtc^{2-} unit for the assembly. Two types of planes are stacked following an ..ABAB.. sequence into a layered structure (Figure 4a). Packing is controlled by the inclusion of GND^+ cations across type A and B layers. They act as H-bond donors to form C=O···H-N and N–H···O-H bonds with the terminal carboxylate groups of the azobenzenetetracarboxylic acid in the neighbouring layers. See Figure SI27 and Table SI6 for H-bond distances. Type B layers (Figure 4b) display a 2D network assembled by the formation of syn-syn ionic H-bond connections equivalent to those in **1,** d(D-A) of 2.427(6) or 2.519(6) Å, for a similar grid-like topology. Empty space in the plane is here occupied by three GND^+ molecules that are linked to the layer by H-bonds with the carboxylic groups pointing inwards the cavity (Figure SI28). As for type A layers, the inclusion of GND^+ is accompanied by water molecules from solution that breaks 2D connectivity. As a result, the lattice is segregated into 1D zig-zag chains whose connectivity is also dictated by H-bonded carboxylic acid dimers between alternative polyaromatic units to produce cavities that are occupied by two GND^+ cations and two water molecules. As shown in Figure SI28, their position within the layer is fixed by a network of supramolecular interactions that involve two H_2O···chain and one H_2O···GND^+ H-bonds. The inclusion of solvent molecules in the cavities seems to be the main factor responsible for disrupting the connectivity in type-A layers. This leads to a distorted packing that precludes the formation of the 1D channels originally present in **1**. TG analyses performed on the solids obtained after the exchange process with GND^+ or $AmGND^+$ showed a similar profile to that of **1** but with two weight loss steps before the total decomposition of the framework, that we ascribed to the loss of DMA^+ and GND^+ or $AmGND^+$ molecules, respectively (Figure SI16,17). To further investigate the reorganization of the supramolecular framework in the presence of GND^+, we repeated the experiments for a handful of crystals with intermittent monitoring in the optical microscope. There is no real retention of single crystallinity and incorporation of the cation can rather

be explained by sequential re-dissolution of **1**, with the solution becoming yellow as result of progressive leaching of H_2abtc^{2-} anions, followed by nucleation and growth of **2** upon incorporation of GND^+ to the structure. The progress of the cation replacement was also monitored by analysing the evolution of the NMR of crystals of **1** soaked in 0.1 M solutions of GND^+ with time (SI2, Table SI1, Figure SI5). Inclusion of GND^+ results in a concomitant decrease of the DMA^+ NMR signal at different time intervals. Equilibrium is achieved after 13 days for an overall substitution percentage of DMA^+ by GND^+ of 84% (Figure 5, dashed lines).

NMR study of DMA replacement with time

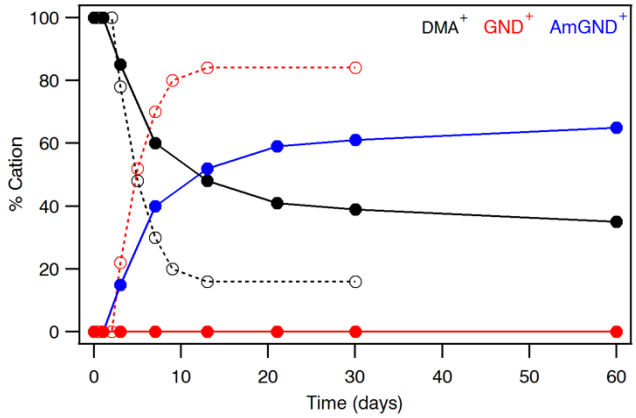

Figure 5. Dynamic replacement of DMA^+ cations in crystals of **1**: soaked in GND^+ [0.1 M] during one month (dashed lines) or in an equimolar mixture of GND^+/$AmGND^+$ [0.05 M] during two months (solid lines). Cation percentages in the sample were extracted from the NMR of dissolved crystals at different time intervals. See SI2 for more details.

For a better understanding of this dynamic cation recognition process, we carried out a similar study by soaking crystals of **1** in 0.05 M equimolar solutions of GND^+ and $AmGND^+$ cations for two months. Monitoring of the reaction by ^1H and ^{13}C NMR at different times (Figures SI7, SI8 and Table SI2) indicates that DMA^+ cations are exclusively replaced with $AmGND^+$ (overall ratio of 65%) with no recognition of GND^+ (Figure 5, solid lines). Unfortunately, we could not isolate single-crystals during the experiment suggesting that the concentration of the cation might play a crucial role in the growth of the $[H_2abtc]^{2-}$ anionic layers upon inclusion of GND^+ or $AmGND^+$ cations. Still, there are several reasons that might justify the preference for $AmGND^+$ from solution. As shown in Figure SI29 $AmGND^+$ offers more H-bond donor and acceptor sites than GND^+ or DMA^+. Furthermore, it is comparatively bigger in size and features richer conformational flexibility. The calculated Van der Waals volumes for DMA^+ and GND^+ display quite close values, 60 and 57 $Å^3$, whereas $AmGND^+$ is close to 15% bigger with 70 $Å^3$. Whilst there are only two conformers accessible for DMA^+ and GND^+, $AmGND^+$ offers a richer conformational landscape with four conformers accessible at the experiment conditions (Figure SI30).[20]

Conclusions

In summary, $[H_2abtc][DMA]_2$ behaves as a chemically adaptable framework capable of undergoing self-organization in the presence of cationic guests like guanidinium and aminoguanidinium. Exposure of the original framework to a concentrated solution of the first results in the spontaneous formation of a new supramolecular architecture from a solution of exchanging components, assisted by reversible formation of labile H-bonds. NMR studies also indicate that this new framework is preferably assembled with aminoguanidium from a mixture of cations likely due to a balance between the size and density of H-bond donor acceptor sites in the cation. This kinetic array cannot be sorted out by crystallization likely due to higher dilution and similar solubility of the interconverting components. This same structural adaptability can be extended to more complex frameworks in which additional chemical functions can be incorporated to guide selective interactions with a broader range of guests.

Conflicts of interest

There are no conflicts to declare.

Acknowledgements

This work was supported by the Spanish MINECO (CTQ2017-83486-P) and the Generalitat Valenciana (GV/2016/137). C.M.-G. and J.C.-G. thank the Spanish MINECO for a Ramón y Cajal Fellowship and FPI Scholarship (CTQ2014-59209-P). N.M.P. thanks the Junta de Andalucía for postdoctoral fellowship P10-FQM-6050.

Notes and references

1 H. Furukawa, K. E. Cordova, M. O'Keeffe and O. M. Yaghi, *Science*, 2013, **341**, 1230444–1230444.
2 N. Huang, P. Wang and D. Jiang, *Nat. Rev. Mater.*, 2016, **1**, 16068.
3 A. M. Beatty, *Coord. Chem. Rev.*, 2003, **246**, 131–143.
4 B. Moulton and M. J. Zaworotko, *Chem. Rev.*, 2001, **101**, 1629–1658.
5 V. A. Russell, C. C. Evans, W. Li and M. D. Ward, *Science*, 1997, **276**, 575–579.
6 P. Brunet, M. Simard and J. D. Wuest, *J. Am. Chem. Soc.*, 1997, **119**, 2737–2738.
7 A. Comotti, S. Bracco, G. Distefano and P. Sozzani, *Chem. Commun.*, 2009, **47**, 284–286.
8 W. Yang, A. Greenaway, X. Lin, R. Matsuda, A. J. Blake, C. Wilson, W. Lewis, P. Hubberstey, S. Kitagawa, N. R. Champness and M. Schröder, *J. Am. Chem. Soc.*, 2010, **132**, 14457–14469.
9 R. V. Afonso, J. Durão, A. Mendes, A. M. Damas and L. Gales, *Angew. Chem. Int. Ed.*, 2010, **49**, 3034–3036.
10 Y. He, S. Xiang and B. Chen, *J. Am. Chem. Soc.*, 2011, **133**, 14570–14573.
11 M. Mastalerz and I. M. Oppel, *Angew. Chem. Int. Ed.*, 2012, **51**, 5252–5255.
12 R. Natarajan, L. Bridgland, A. Sirikulkajorn, J.-H. Lee, M. F. Haddow, G. Magro, B. Ali, S. Narayanan, P. Strickland, J. P. H.

Charmant, A. G. Orpen, N. B. McKeown, C. G. Bezzu and A. P. Davis, *J. Am. Chem. Soc.*, 2013, **135**, 16912–16925.
13 P. Li, Y. He, H. D. Arman, R. Krishna, H. Wang, L. Weng and B. Chen, *Chem. Commun.*, 2014, **50**, 13081–13084.
14 T.-H. Chen, I. Popov, W. Kaveevivitchai, Y.-C. Chuang, Y.-S. Chen, O. Daugulis, A. J. Jacobson and O. Š. Miljanić, *Nat. Commun.*, 2014, **5**, 5131.
15 H. Wang, Bin Li, H. Wu, T.-L. Hu, Z. Yao, W. Zhou, S. Xiang and B. Chen, *J. Am. Chem. Soc.*, 2015, **137**, 9963–9970.
16 R. S. Patil, D. Banerjee, C. Zhang, P. K. Thallapally and J. L. Atwood, *Angew. Chem. Int. Ed.*, 2016, **55**, 4523–4526.
17 S. Ameerunisha and P. S. Zacharias, *Journal of the Chemical Society, Perkin Transactions 2*, 1995, 1679–1682.
18 A. Dhakshinamoorthy, M. Alvaro, H. Chevreau, P. Horcajada, T. Devic, C. Serre and H. García, *Catal. Sci. Technol.*, 2012, **2**, 324–330.
19 O. V. Dolomanov, L. J. Bourhis, R. J. Gildea, J. A. K. Howard and H. Puschmann, *J. Appl. Cryst.*, 2009, **42**, 339–341.
20 G. M. Sheldrick, *Acta Crystallogr A Found Adv*, 2015, **71**, 3–8.
21 G. M. Sheldrick, *Acta Crystallogr C Struct Chem*, 2015, **71**, 3–8.
22 S. A. Dalrymple and G. K. H. Shimizu, *J. Am. Chem. Soc.*, 2007, **129**, 12114–12116.
23 P. Dechambenoit, S. Ferlay, N. Kyritsakas and M. W. Hosseini, *J. Am. Chem. Soc.*, 2008, **130**, 17106–17113.
24 N. Roques, G. Mouchaham, C. Duhayon, S. Brandès, A. Tachon, G. WEBER, J. P. Bellat and J.-P. Sutter, *Chem-Eur J.*, 2014, **20**, 11690–11694.
25 G. Mouchaham, N. Roques, W. Khodja, C. Duhayon, Y. Coppel, S. Brandès, T. Fodor, M. Meyer and J.-P. Sutter, *Chem-Eur J.*, 2017, **23**, 11818–11826.
26 C.-L. Chen and A. M. Beatty, *J. Am. Chem. Soc.*, 2008, **130**, 17222–17223.
27 K. Biradha, D. Dennis, V. A. MacKinnon, C. V. Krishnamohan Sharma and M. J. Zaworotko, *J. Am. Chem. Soc.*, 1998, **120**, 11894–11903.
28 W. Xiao, C. Hu and M. D. Ward, *J. Am. Chem. Soc.*, 2014, **136**, 14200–14206.
29 Y. Marcus, *Chem. Soc. Rev.*, 1993, **22**, 409–416.
30 D. Dumitrescu, Y. M. Legrand, F. Dumitrascu, M. Barboiu and A. Van Der Lee, *Cryst. Growth Des.*, 2012, **12**, 4258–4263.

